

Numerical Heat Transfer, Part B: Fundamentals: An International Journal of Computation and Methodology

Publication details, including instructions for authors and
subscription information:

<http://www.tandfonline.com/loi/unhb20>

A Reference Benchmark Solution for Free Convection in A Square Cavity Filled with A Heterogeneous Porous Medium

Marwan Fahs ^a, Anis Younes ^a & Ahmed Makradi ^b

^a Laboratoire d'Hydrologie et Géochimie de Strasbourg, University of Strasbourg, CNRS, UMR 7517, Strasbourg, France

^b Luxembourg Institute of Science and Technology, LIST, Luxembourg

Published online: 26 Feb 2015.



CrossMark

[Click for updates](#)

To cite this article: Marwan Fahs, Anis Younes & Ahmed Makradi (2015) A Reference Benchmark Solution for Free Convection in A Square Cavity Filled with A Heterogeneous Porous Medium, Numerical Heat Transfer, Part B: Fundamentals: An International Journal of Computation and Methodology, 67:5, 437-462, DOI: [10.1080/10407790.2014.977183](https://doi.org/10.1080/10407790.2014.977183)

To link to this article: <http://dx.doi.org/10.1080/10407790.2014.977183>

PLEASE SCROLL DOWN FOR ARTICLE

Taylor & Francis makes every effort to ensure the accuracy of all the information (the "Content") contained in the publications on our platform. However, Taylor & Francis, our agents, and our licensors make no representations or warranties whatsoever as to the accuracy, completeness, or suitability for any purpose of the Content. Any opinions and views expressed in this publication are the opinions and views of the authors, and are not the views of or endorsed by Taylor & Francis. The accuracy of the Content should not be relied upon and should be independently verified with primary sources of information. Taylor and Francis shall not be liable for any losses, actions, claims, proceedings, demands, costs, expenses, damages, and other liabilities whatsoever or howsoever caused arising directly or indirectly in connection with, in relation to or arising out of the use of the Content.

This article may be used for research, teaching, and private study purposes. Any substantial or systematic reproduction, redistribution, reselling, loan, sub-licensing, systematic supply, or distribution in any form to anyone is expressly forbidden. Terms &

A REFERENCE BENCHMARK SOLUTION FOR FREE CONVECTION IN A SQUARE CAVITY FILLED WITH A HETEROGENEOUS POROUS MEDIUM

Marwan Fahs¹, Anis Younes¹, and Ahmed Makradi²

¹Laboratoire d'Hydrologie et de Géochimie de Strasbourg, University of Strasbourg, CNRS, UMR 7517, Strasbourg, France

²Luxembourg Institute of Science and Technology, LIST, Luxembourg

The Fourier-Galerkin (FG) method is used to produce a highly accurate solution for free convection in a square cavity filled with heterogeneous porous medium. To this end, the governing equations are reformulated in terms of the temperature and the stream function. These unknowns are then expanded in infinite Fourier series truncated at given orders. The accuracy of the FG solution is investigated for different truncation orders and compared to the results of an advanced finite-element numerical model using fine-mesh discretization. The obtained results represent a set of high-quality data that can be used for benchmarking numerical models.

1. INTRODUCTION

Free-convection heat transfer in fluid-saturated porous media is encountered in a broad spectrum of industrial, environmental, and engineering applications. This covers, for example, buildings insulation, chemical reactors, post-accident heat removal in nuclear reactors, PEM fuel cell operation, and some geophysical problems such as frost heaves, geothermal energy production, and underground storage of nuclear waste. A review of the applications of free convection in porous media is provided by Ingham and Pop [1] and Nield and Bejan [2]. The problem has been widely studied in recent decades ([1–4] and references therein). Special attention is given to the free convection in heterogeneous porous media [5–23] because the nonuniformity of the permeability and/or the thermal diffusivity significantly affects the overall rate of heat transfer. The effect of heterogeneity is especially important in geothermal applications because hydraulic properties, such as permeability, can vary by several orders of magnitude over small spatial scales [7, 9, 17, 24, 25].

The effect of heterogeneity has been studied for both external and internal natural convection using different heterogeneity configurations (stratified, horizontal, vertical, random, and periodic) [5–23]. For internal natural convection two situations, with either heating from below or from the sides, were examined ([11] and

Received 24 April 2014; accepted 4 September 2014.

Address correspondence to Marwan Fahs, LHYGES, 1 rue Blessig, 67084, Strasbourg, France.
E-mail: fahs@unistra.fr

NOMENCLATURE

A	stream function coefficients	X	dimensionless horizontal coordinate $(=x/L)$
B	temperature coefficients	z	vertical coordinate
g	acceleration due to gravity	Z	dimensionless vertical coordinate $(=z/L)$
k	permeability	α	effective thermal diffusivity
k_0	permeability at the origin	β	coefficient of thermal expansion of fluid
\bar{k}	average permeability	γ	matrix coefficient [Eq. (24)]
L	cavity square side	Γ	matrix coefficient [Eq. (23)]
N_c	total number of Fourier coefficients	δ	Kronecker delta function
N_e	total number of mesh elements	ΔT	temperature difference
N_m	stream function truncation order in X	ε	ratio of composite material to convective fluid heat capacities
N_n	stream function truncation order in Z	ς	rate of change of the permeability in x
N_r	temperature truncation order in X	η	temperature change of variable [Eq. (15)]
N_s	temperature truncation order in Z	θ	dimensionless temperature $[=(T - T_c)/\Delta T]$
N_u	local Nusselt number	λ	matrix coefficient [Eq. (24)]
\bar{N}_u	average Nusselt number	Λ	trial function for heat transfer equation
p	pressure	μ	fluid viscosity
R_a	local Rayleigh number $(=kL\beta g\rho_c \Delta T/\mu\alpha)$	ξ	matrix coefficient [Eq. (24)]
R_{a0}	Rayleigh at origin $(=k_0 L \beta g \rho_c \Delta T / \mu \alpha)$	ρ	fluid density
\overline{R}_a	average Rayleigh number	Π	matrix coefficient [Eq. (24)]
R^F	flow equation residual	σ	rate of change of the permeability in z
R^H	heat transfer equation residual	τ	matrix coefficient [Eq. (24)]
t	time	Ψ	dimensionless stream function
T	temperature	ϕ	stream function
u	velocity component in the x direction	Φ	trial function for the flow equation
U	dimensionless velocity component in the x direction $(=uL/\alpha)$	ω	vector coefficient [Eq. (24)]
U^{\max}	dimensionless maximum horizontal velocity at the mid-plane $X=0.5$	Ω	matrix coefficient [Eq. (23)]
v	velocity component in the z direction		
V	dimensionless velocity component in the z direction $(=vL/\alpha)$		
V^{\max}	dimensionless maximum vertical velocity at the mid-plane $Z=0.5$		
x	horizontal coordinate		
			Subscripts and Superscripts
		c	cold fluid
		h	hot fluid

references therein). Due to the complexity of the physical processes, the problem of free convection in saturated porous media is often investigated numerically. In this context, several models and simulators that are capable of solving the governing equations numerically have been developed and used in the literature [25–40]. However, despite the significant amounts of effort spent on this topic, to the authors' best knowledge, there is no reference benchmark solution that allows the validation of numerical codes in the case of heterogeneous porous media. Indeed, the numerical results are generally validated by comparison among various published numerical results, based on a variety of numerical models [39]. However, this comparison often involves some discrepancies. The matching between the numerical results is rarely perfect because of the different approximations used in the numerical codes when

solving highly nonlinear problems. Therefore, there is a clear need for highly accurate reference benchmark solutions that can be used specifically for validation purposes. This is why we propose an accurate benchmark reference solution for free convection in saturated heterogeneous porous media in this study.

The considered benchmark is the popular square cavity filled with a saturated porous medium and subject to differentially heated vertical walls and adiabatic horizontal surfaces [26, 27, 30, 33, 35, 37–39]. The simplicity of the geometry and the boundary conditions renders this problem especially suitable for testing numerical models. The porous medium is considered to be heterogeneous where, for convenience, the permeability is assumed to vary exponentially with respect to the spatial directions. Under these conditions, a highly accurate steady-state solution is investigated using the Fourier-Galerkin method (FG) [41–51].

The FG method is a spectral method usually used to accurately solve partial differential equations (PDEs) ([42, 49] and references therein). Spectral methods are used extensively in large-scale computations in meteorology, magnetohydrodynamics, and turbulent flows [47, 52]. The main idea of spectral methods is to expand the unknowns into appropriate infinite series truncated at given orders. Therefore, the sole generated error with these methods is due to the truncation of the series expansion [42, 51]. The obtained solution is considered to be exact if the truncation order tends to infinity [53]. The rate of convergence of the spectral methods depends only on the smoothness of the solution, yielding the ability to achieve high precision with a relatively small number of degrees of freedom [49]. Among several spectral methods, the FG method is chosen here because of its simplicity, popularity, and fast algorithm [51, 54]. The FG method is developed for the stream function–temperature form of the governing equations. This leads to a highly nonlinear system of algebraic equations that we solved with an efficient algorithm based on the modified Powell hybrid method [55–57]. To reduce the computational effort of this algorithm, the Jacobian matrix is evaluated analytically instead of through a finite-difference approximation. The major drawback of the FG method is its impractical use in the presence of nonlinearity, which induces fairly complex summations that resemble a convolution [43, 49]. However, this study shows that this difficulty might be circumvented in the porous-cavity problem because terms involving four overlapped summations can be reduced to only double sums.

The results of the FG method are then validated against the results of an advanced finite-element (FE) model. This model was developed by Younes et al. [58] to simulate solute transfer in saturated porous media. It is adapted here for thermal diffusion. The FE model uses advanced and appropriate numerical schemes for both time integration and spatial discretization. The time integration is performed via the method of lines (MOL) to achieve high temporal accuracy. The spatial discretization is performed using a combination of the mixed finite-element (MFE), discontinuous Galerkin (DG), and multipoint flux approximation (MPFA) methods to achieve high accuracy for each type of equation. This combination was shown to be accurate and robust for modeling density-driven flow problems [50, 59]. To improve the quality of the new benchmark solution, the comparison between the FG and FE solutions is performed by considering several quantities of interest, such as the streamlines, isotherms, velocity field, and Nusselt number.

The article is organized as follows. Section 2 is devoted to the description of the benchmark problem and the governing equations. Sections 3 and 4 are devoted to

the development of the FG and FE solutions, respectively. In Section 5, the FG and FE solutions are presented and discussed for homogenous and vertically and horizontally heterogenous porous media. Finally, a summary and conclusion are given in Section 6.

2. BENCHMARK DESCRIPTION AND GOVERNING EQUATIONS

We considered a square enclosure filled with a fluid-saturated heterogeneous porous medium. The left and right vertical walls are maintained at constant temperatures T_h and T_c ($T_h > T_c$), respectively. The horizontal surfaces are assumed to be adiabatic (Figure 1). We made the following assumptions: The properties of the fluid and the porous medium are constant, the inertia and the viscous drag are negligible, the fluid and the porous medium are locally in thermal equilibrium, and the Darcy and Boussinesq approximations are valid. Under these conditions, the fluid flow in the porous cavity can be modeled using the continuity equation and Darcy's law written as follows (Mahmud and Pop [60]):

$$\frac{\partial u}{\partial x} + \frac{\partial v}{\partial z} = 0 \quad (1)$$

$$u = -\frac{k}{\mu} \frac{\partial p}{\partial x} \quad (2)$$

$$v = -\frac{k}{\mu} \left(\frac{\partial p}{\partial z} + \rho g \right) \quad (3)$$

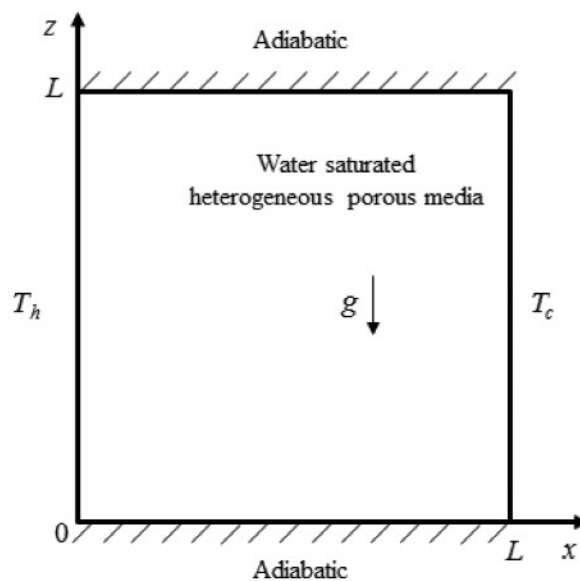


Figure 1. Schematic diagram of the heterogeneous porous-cavity problem.

where u and v are the velocity components in the x and z directions, $k = k(x, z)$ is the permeability assumed to be a function of x and z , and p , ρ , μ , and g are, respectively, the pressure, density, viscosity, and gravity.

The heat transfer inside the cavity is modeled using the energy equation written as

$$\varepsilon \frac{\partial T}{\partial t} + u \frac{\partial T}{\partial x} + v \frac{\partial T}{\partial z} = \alpha \left(\frac{\partial^2 T}{\partial x^2} + \frac{\partial^2 T}{\partial z^2} \right) \quad (4)$$

where ε is the ratio of the composite material heat capacity to the convective fluid heat capacity and T , t , and α are, respectively, the temperature, time, and effective thermal diffusivity.

The density is assumed to vary with temperature as a first-order polynomial,

$$\rho = \rho_c [1 - \beta(T - T_c)] \quad (5)$$

where ρ_c is the density of the fluid at the cold temperature (T_c) and β is the coefficient of thermal expansion.

The governing steady-state equations can be reformulated in terms of the stream function and the temperature, with the stream function ϕ defined by

$$u = \frac{\partial \phi}{\partial z} \quad v = -\frac{\partial \phi}{\partial x} \quad (6)$$

The pressure can be eliminated from the Darcy's law equations by differentiating Eqs. (2) and (3) with respect to z and x , respectively, and by subtracting the resulting equations each from other. Using Eqs. (2), (3), and (6), the final equation can be written as

$$\frac{\partial^2 \phi}{\partial x^2} + \frac{\partial^2 \phi}{\partial z^2} = -\frac{kg\beta\rho_c}{\mu} \frac{\partial T}{\partial x} + \frac{1}{k} \frac{\partial k}{\partial x} \frac{\partial \phi}{\partial x} + \frac{1}{k} \frac{\partial k}{\partial z} \frac{\partial \phi}{\partial z} \quad (7)$$

Using Eqs. (6), the temperature-stream function form of the steady-energy equation can be written as follows:

$$\frac{\partial \phi}{\partial z} \frac{\partial T}{\partial x} - \frac{\partial \phi}{\partial x} \frac{\partial T}{\partial z} = \alpha \left(\frac{\partial^2 T}{\partial x^2} + \frac{\partial^2 T}{\partial z^2} \right) \quad (8)$$

The dimensionless form of Eqs. (7) and (8) is obtained using the following dimensionless variables:

$$\psi = \frac{\phi}{\alpha} \quad \theta = \frac{T - T_c}{\Delta T} \quad X = \frac{x}{L} \quad Z = \frac{z}{L} \quad (9)$$

where L is the cavity side and $\Delta T = T_h - T_c$ is the temperature difference between the hot and cold walls.

Equations (7) and (8) then take the following form:

$$\frac{\partial^2 \psi}{\partial X^2} + \frac{\partial^2 \psi}{\partial Z^2} = -Ra \frac{\partial \theta}{\partial X} + \frac{1}{k} \frac{\partial \psi}{\partial X} \frac{\partial k}{\partial X} + \frac{1}{k} \frac{\partial \psi}{\partial Z} \frac{\partial k}{\partial Z} \quad (10)$$

$$\frac{\partial \psi}{\partial Z} \frac{\partial \theta}{\partial X} - \frac{\partial \psi}{\partial X} \frac{\partial \theta}{\partial Z} = \left(\frac{\partial^2 \theta}{\partial X^2} + \frac{\partial^2 \theta}{\partial Z^2} \right) \quad (11)$$

where Ra is the local Rayleigh number defined by

$$Ra = \frac{kL\beta g\rho_c \Delta T}{\mu\alpha} \quad (12)$$

The dimensionless temperature–stream function equations [Eqs. (10) and (11)] are subjected to the following boundary conditions:

$$\psi(0, Z) = \psi(1, Z) = \psi(X, 0) = \psi(X, 1) = 0 \quad (13)$$

$$\theta(0, Z) = 1 \quad \theta(1, Z) = 0 \quad \partial \theta(X, 0)/\partial Z = \partial \theta(X, 1)/\partial Z = 0 \quad (14)$$

3. THE FOURIER-GALERKIN SOLUTION

The FG method requires periodic boundary conditions. This can be obtained using the following change of variable:

$$\eta = \theta + X - 1 \quad (15)$$

Therefore, Eqs. (10) and (11) take the form

$$\frac{\partial^2 \psi}{\partial X^2} + \frac{\partial^2 \psi}{\partial Z^2} - \frac{1}{k} \frac{\partial \psi}{\partial X} \frac{\partial k}{\partial X} - \frac{1}{k} \frac{\partial \psi}{\partial Z} \frac{\partial k}{\partial Z} + Ra \frac{\partial \eta}{\partial X} - Ra = 0 \quad (16)$$

$$\left(\frac{\partial^2 \eta}{\partial X^2} + \frac{\partial^2 \eta}{\partial Z^2} \right) - \frac{\partial \psi}{\partial Z} \frac{\partial \eta}{\partial X} + \frac{\partial \psi}{\partial Z} + \frac{\partial \psi}{\partial X} \frac{\partial \eta}{\partial Z} = 0 \quad (17)$$

with the following periodic boundary conditions:

$$\psi(0, Z) = \psi(1, Z) = \psi(X, 0) = \psi(X, 1) = 0 \quad (18)$$

$$\eta(0, Z) = \eta(1, Z) = 0 \quad \partial \eta(X, 0)/\partial Z = \partial \eta(X, 1)/\partial Z = 0 \quad (19)$$

The stream function ψ and the temperature η are then expanded using Fourier series as follows:

$$\psi = \sum_{m=1}^{Nm} \sum_{n=1}^{Nn} A_{m,n} \sin(m\pi Z) \sin(n\pi X) \quad (20)$$

$$\eta = \sum_{r=0}^{Nr} \sum_{s=1}^{Ns} B_{r,s} \cos(r\pi Z) \sin(s\pi X) \quad (21)$$

where Nm and Nn (resp. Nr and Ns) are the truncation orders for the stream function (resp. temperature) in the x and z directions and $A_{m,n}$ and $B_{r,s}$ are the Fourier series coefficients for the stream function and the temperature, respectively.

Note that the boundary conditions Eqs. (18) and (19) are identically verified by the expansions Eqs. (20) and (21).

Equations (20) and (21) are then substituted into Eqs. (16) and (17) and the resulting equations are multiplied, respectively, by $\Phi_{g,h}=4\sin(g\pi Z)\sin(h\pi X)$ for ($g=1..Nm$, $h=1..Nn$) and $\Lambda_{g,h}=4\cos(g\pi Z)\sin(h\pi X)$ for ($g=0..Nr$, $h=1..Ns$) and integrated over the square domain.

The porous medium is assumed to be heterogeneous with the following permeability distribution:

$$k(X, Z) = k_0 e^{\zeta L X + \sigma L Z} \quad (22)$$

where k_0 is the permeability at the origin ($X=Z=0$) and ζ and σ are the rates of change of $\ln(k)$ in the x and z directions, respectively.

The exponential distribution of the permeability is adopted to allow analytical evaluation of all the double integrals arising with the FG method. In addition, this distribution is useful for examining the homogenous case ($\zeta=0$, $\sigma=0$) and the vertical ($\zeta \neq 0$, $\sigma=0$) and horizontal ($\zeta=0$, $\sigma \neq 0$) heterogeneous stratifications.

The FG method with Eq. (22) leads to the following set of nonlinear algebraic equations with $A_{g,h}$ and $B_{g,h}$ as unknowns:

$$\begin{aligned} R_{g,h}^F = & -\pi^2(h^2 + g^2)A_{g,h} - \zeta L \sum_{n=1}^{Nn} n A_{g,n} \Gamma_{h,n} - \sigma L \sum_{m=1}^{Nm} m A_{m,h} \Gamma_{g,m} \\ & + \pi^3 \text{Ra}_0 \sum_{r=0}^{Nr} \sum_{s=1}^{Ns} s B_{r,s} \Omega_{g,r}^\sigma \Omega_{h,s}^\zeta - \text{Ra}_0 \Omega_{g,0}^\sigma \Omega_{h,0}^\zeta = 0 \end{aligned} \quad (23)$$

for ($g=1..Nm$, $h=1..Nn$)

$$\begin{aligned} R_{g,h}^H = & -\omega_g \pi^2(h^2 + g^2)B_{g,h} + \pi g \Pi_{g,h} \\ & - \frac{\pi^2}{4} \sum_{m=1}^{Nm} \sum_{n=1}^{Nn} \sum_{r=0}^{Nr} \sum_{s=1}^{Ns} A_{m,n} B_{r,s} (m.s.\gamma_{g,m,r}\lambda_{h,n,s} + n.r.\tau_{g,m,r}\xi_{h,n,s}) = 0 \end{aligned} \quad (24)$$

for ($g=0..Nr$, $h=1..Ns$)

where R^F and R^H are the residuals corresponding to Eqs. (16) and (17), respectively and Ra_0 is the Rayleigh number at the origin, defined by

$$\text{Ra}_0 = \frac{k_0 L \beta g \rho_c \Delta T}{\mu \alpha} \quad (25)$$

The coefficients γ , λ , τ , ω , and ξ in Eq. (24) are given by

$$\gamma_{g,m,r} = \delta_{g,m-r} + \delta_{g,r-m} + \delta_{g,m+r}\lambda_{h,n,s} = \delta_{h,n+s} + \delta_{h,n-s} - \delta_{h,s-n} \quad (26)$$

$$\tau_{g,m,r} = \delta_{g,r-m} + \delta_{g,m-r} - \delta_{g,m+r}\xi_{h,n,s} = \delta_{h,n+s} - \delta_{h,n-s} + \delta_{h,s-n} \quad (27)$$

$$\omega_g = \begin{cases} 1 & \text{if } g \neq 0 \\ 2 & \text{if } g = 0 \end{cases} \quad (28)$$

The matrices Γ , Ω^σ , Ω^ζ , and Π in Eqs. (23) and (24) are given by

$$\Gamma_{i,j} = \begin{cases} \left[\frac{1-(-1)^{i+j}}{i+j} + \frac{1-(-1)^{i-j}}{i-j} \right] & \text{if } i \neq j \\ 0 & \text{if } i = j \end{cases} \quad (29)$$

$$\Omega_{i,j}^\sigma = \begin{cases} \left((i+j) \frac{1-(-1)^{i+j} e^{L\sigma}}{L^2 \sigma^2 + (i+j)^2 \pi^2} + (i-j) \frac{1-(-1)^{i-j} e^{L\sigma}}{L^2 \sigma^2 + (i-j)^2 \pi^2} \right) & \text{if } i \neq j \\ 0 & \text{if } i = j \end{cases} \quad (30)$$

$$\Omega_{i,j}^\zeta = \begin{cases} \left((i+j) \frac{1-(-1)^{i+j} e^{L\zeta}}{L^2 \zeta^2 + (i+j)^2 \pi^2} + (i-j) \frac{1-(-1)^{i-j} e^{L\zeta}}{L^2 \zeta^2 + (i-j)^2 \pi^2} \right) & \text{if } i \neq j \\ 0 & \text{if } i = j \end{cases} \quad (31)$$

$$\Pi_{i,j} = \begin{cases} A_{i,j} & 1 \leq i \leq Nm \text{ and } 1 \leq j \leq Nn \\ 0 & \text{elsewhere} \end{cases} \quad (32)$$

where $\delta_{i,j}$ is the Kronecker delta function.

Equations (23) and (24) form a system of $Nm \times Nn + (Nr+1) \times Ns$ nonlinear equations. This system is solved here using an efficient nonlinear solver from the IMSL library [61]. The solver is based on the modified Powell hybrid algorithm, which is an improved Newton's method [55–57]. The algorithm estimates the correction using a convex combination of the Newton method and scaled gradient directions and as well as the approach of the generalized trust region. The Jacobian matrix is approximated from iteration to iteration by the rank-one method [62]. Thus, the entire Jacobian is calculated only at the first iteration or when two successive attempts have failed to reduce the residual. The solver allows for a numerical (finite difference) or analytical user-supplied calculation of the Jacobian matrix. In this study, the algorithm is supplied with the analytical Jacobian matrix to improve the convergence and to reduce the computational effort. For this purpose, the residuals R^F and R^H are differentiated with respect to the coefficients $A_{i,j}$ and $B_{i,j}$ as follows:

$$\frac{\partial R_{g,h}^F}{\partial A_{i,j}} = -\pi^2 (i^2 + j^2) \delta_{i,g} \delta_{j,h} - L (\zeta j \Gamma_{h,j} + \sigma i \Gamma_{g,i}) \quad (33)$$

$$\frac{\partial R_{g,h}^F}{\partial B_{i,j}} = \pi^3 \text{Ra}_0 j \Omega_{g,i}^\sigma \Omega_{h,j}^\zeta \quad (34)$$

$$\frac{\partial R_{g,h}^H}{\partial A_{i,j}} = \pi g \delta_{i,g} \delta_{j,h} - \frac{\pi^2}{4} \sum_{r=0}^{Nr} \sum_{s=1}^{Ns} B_{r,s} (i.s. \gamma_{g,i,r} \lambda_{h,j,s} + j.r. \tau_{g,i,r} \xi_{h,j,s}) \quad (35)$$

$$\frac{\partial R_{g,h}^H}{\partial B_{i,j}} = -\omega_g \pi^2 (i^2 + j^2) \delta_{i,g} \delta_{j,h} - \frac{\pi^2}{4} \sum_{m=1}^{Nm} \sum_{n=1}^{Nn} A_{m,n} (m.j. \gamma_{g,m,i} \lambda_{h,n,j} + n.i. \tau_{g,m,i} \xi_{h,n,j}) \quad (36)$$

Note that the computation of the FG solution quickly becomes very expensive (or even impractical) for problems with high Rayleigh numbers that require a large number of Fourier coefficients. This is caused by the term of four overlapped summations in Eq.(24). To avoid this problem, we show in the Appendix how the most expansive term involving four overlapped summation can be simplified to only double-overlapped summations. Thus, the evaluation of this term reduces from $O(Nm \times Nn \times Nr \times Ns)$ operations to $O(4 \times Nr \times Ns)$ operations.

4. THE FINITE-ELEMENT NUMERICAL MODEL

The FE model, developed by Younes et al. [58], is used here to simulate coupled flow and heat transfer. The model provides accurate solutions by using advanced and appropriate techniques for both time integration and spatial discretization.

For the spatial discretization, a specific method is used to achieve high accuracy for each type of equation. Thus, the MFE method is used for the discretization of the flow equation. This method produces accurate and consistent velocity fields even for highly heterogeneous domains [63, 64]. The heat transfer equation is discretized through a combination of DG and MPFA methods [59]. The DG method is used for the convective part because it provides robust and accurate numerical solutions for problems involving steep fronts [65]. The MPFA method is used for the diffusive part because it allows for the handling of anisotropic heterogeneous domains and can be easily combined with the DG method [59, 66].

The time discretization is performed via the MOL, which is a technique for improving temporal accuracy when solving PDEs through the use of adaptive higher-order time integration schemes with formal error controls. With the MOL, we first discretize the spatial derivatives and subsequently integrate in time the semi-discrete problem as a system of ODEs. In this study, the ODE system is solved using the DLSODIS solver, which is a variable time, variable order of ODE solver [67–70]. The solver adapts both the time step-size and the order of time integration to obtain the prescribed accuracy.

5. RESULTS AND DISCUSSION

In this section, highly accurate FG reference solutions are investigated for free convection in heterogeneous porous media and compared with the FE model results. Three configurations are studied: homogeneous and vertical and horizontal heterogeneous stratifications. The same average permeability \bar{k} is used for all the configurations. This average is defined as follow

$$\bar{k} = \int_0^1 \int_0^1 k(X, Z) dX dZ \quad (37)$$

For each configuration, the reference solution is calculated for three values of the average Rayleigh number (10^2 , 10^3 , and 10^4). The average Rayleigh number is calculated based on the average permeability and is defined as follows:

$$\overline{\text{Ra}} = \frac{\bar{k} L \beta g \rho_c \Delta T}{\mu \alpha} \quad (38)$$

The dimensional parameters that were used to generate these values of the average Rayleigh number are listed in Table 1.

The accuracy of the FG and FE solutions is assessed regarding several quantities related to the flow and heat transfer processes. As is customary for porous-cavity problems, the assessment of the flow process is based on the streamlines and the maximum values of the dimensionless horizontal velocity U^{\max} at the mid-plane $X=0.5$ and that of the vertical velocity V^{\max} at the mid-plane $Z=0.5$. The velocities are made dimensionless as follows:

$$U = \frac{uL}{\alpha} \quad V = \frac{vL}{\alpha} \quad (39)$$

For the heat transfer process, the assessment is based on the principal (0.2, 0.4, 0.6 and 0.8) isotherms and the average Nusselt number:

$$\overline{\text{Nu}} = \int_0^1 \text{Nu} dZ \quad (40)$$

where Nu is the local Nusselt number defined by

Table 1. Parameters used for all test cases

Cavity square side	$L = 1\text{m}$
Average permeability	$\bar{k} = 10^{-9}\text{m}^2$
Ratio of heat capacity	$\epsilon = 1$
Thermal diffusivity (for $\overline{\text{Ra}} = 10^2$)	$\alpha = 10^{-6} \text{ m}^2\text{s}$
Thermal diffusivity (for $\overline{\text{Ra}} = 10^3$)	$\alpha = 10^{-7} \text{ m}^2\text{s}$
Thermal diffusivity (for $\overline{\text{Ra}} = 10^4$)	$\alpha = 10^{-8} \text{ m}^2\text{s}$
Density of the fluid at the cold temperature	$\rho_c = 1,000\text{kg/m}^3$
Coefficient of thermal expansion	$\beta = 0.01$
Gravity	$g = 10\text{m/s}^2$
Viscosity	$\mu = 10^{-3} \text{ kg.m.s}$
Cold-wall temperature	$T_c = 0^\circ\text{C}$
Hot-wall temperature	$T_h = 1^\circ\text{C}$

$$\text{Nu} = \frac{\partial \theta}{\partial X} \Big|_{X=0} \quad (41)$$

Note that with the FG method, the average Nusselt number can be expressed analytically using the Fourier expansion of the temperature as follows:

$$\overline{\text{Nu}} = \pi \sum_{s=1}^{Ns} s B_{0,s} - 1 \quad (42)$$

For all the studied test cases, the FG solution is investigated using several levels of truncation orders to ensure the stability and accuracy of the reference solution. Furthermore, the FE solution is investigated using different levels of mesh refinement to ensure a mesh-independent solution. Different triangular meshes are used by subdividing square elements into four equal triangles (by connecting the center of the square to its four nodes). The FE simulations are performed until a long non-dimensional time has elapsed to ensure steady-state solutions.

In the following, the convergence of the FG (resp. FE) solution is assumed to be reached when all the quantities of interest (the streamlines, isotherms, average Nusselt number and the maximum velocities) become relatively insensitive to the truncation order (resp. to the mesh refinement).

5.1. Homogenous Cavity

In this section, the porous medium is assumed to be homogenous ($\zeta = \sigma = 0$) with a constant permeability $\bar{k} = 10^{-9}\text{m}^2$ (see Table 1). The FG solution is investigated for three values of the average Rayleigh number ($\overline{\text{Ra}} = 10^2$, 10^3 , and 10^4). The results show that for the low average Rayleigh number ($\overline{\text{Ra}} = 10^2$), the stable FG solution is obtained with the following truncation orders: $Nm = 30$, $Nr = 29$, and $Nm = Ns = 50$. Indeed, in this case, heat transfer in the cavity is largely affected by the diffusion processes and much less by the buoyancy forces. Hence, the steady-state solution is relatively smooth, and a relatively small number of Fourier coefficients is required to obtain the converged solution. For higher average Rayleigh number, the buoyancy effect becomes more important and the solution becomes steeper. Hence, a large number of Fourier coefficients is required for the converged solution. In these cases, the converged solution is obtained with $Nm = 80$, $Nr = 79$, and $Nm = Ns = 100$ for $\overline{\text{Ra}} = 10^3$, while it is obtained with $Nm = 160$, $Nr = 159$, and $Nm = Ns = 225$ for $\overline{\text{Ra}} = 10^4$.

Note that the computation of the FG solutions with a large number of Fourier coefficients was made possible because of the following simplifications:

1. Only half of the Fourier coefficients are computed for each of the previous test cases because the coefficients $A_{i,j}$ and $B_{i,j}$ are identically equal to zero if $(i+j)$ is even. This simplification is valid only in the case of homogeneous porous media.
2. The use of the analytical evaluation of the Jacobian matrix. For instance, the finite-difference evaluation of the Jacobian matrix in the case of 3,000 Fourier

Table 2. FG results in the case of homogenous porous media (Nc -the total number of Fourier coefficients)

$\overline{\text{Ra}}$	Nc	$\overline{\text{Nu}}$	U^{\max}	V^{\max}
10^2	1,500	3.11	17.46	35.94
10^3	8,000	13.38	74.65	414.83
10^4	36,000	46.14	318.44	4,608.54

coefficients requires more than one day of CPU time, whereas the same matrix can be calculated analytically in 15 s.

3. The reduction of the last term in Eq. (24) involving four overlapped summations to four terms each involving a double overlapped summation. For instance, the evaluation of the residual with four overlapped summations in the case of 36,000 Fourier coefficients requires 324×10^6 operations. This takes more than three days of CPU time. The evaluation of the same term with the simplified form requires 18,000 operations and takes only 10 s of CPU time.

The results of the FG method are summarized in Table 2. This table provides the effective number of Fourier coefficients (Nc) used in the converged FG solutions as well as the corresponding values of the average Nusselt number and the maximum velocities for the three test cases corresponding to $\overline{\text{Ra}} = 10^2$, 10^3 , and 10^4 .

The three homogenous test cases corresponding to $\overline{\text{Ra}} = 10^2$, 10^3 , and 10^4 are subsequently simulated with the FE numerical model. Table 3 provides the number of mesh elements used to obtain the converged FE solution as well as the values of the average Nusselt number and the maximum velocities for each test case.

The results show that, for the small average Rayleigh number, the converged FE solution is obtained with a relatively large coarse mesh involving 10,000 elements. For the higher average Rayleigh number, the buoyancy effect becomes more significant. Thus, finer mesh should be used to obtain the converged solution (22,500 elements for $\overline{\text{Ra}} = 10^3$ and 90,000 elements for $\overline{\text{Ra}} = 10^4$).

The converged FG and FE solutions are subsequently compared regarding the maximum velocities, average Nusselt number, streamlines, and isotherms. Very nearly converged maximum velocities and average Nusselt numbers are observed in Tables 2 and 3. For all the Rayleigh numbers, the difference between the FG and the FE results is less than 3%.

The streamlines and the isotherms are plotted in Figure 2. This figure shows excellent agreement between the FG and the FE results for all the Rayleigh numbers. For $\overline{\text{Ra}} = 10^2$, the heat enters the domain from the left side to the right side. The density effects generate a clockwise circulating flow with a relatively slow motion

Table 3. FE results in the case of homogenous porous media (Ne -total number of mesh elements)

$\overline{\text{Ra}}$	Ne	$\overline{\text{Nu}}$	U^{\max}	V^{\max}
10^2	10,000	3.10	17.42	35.82
10^3	22,500	13.48	74.66	409.95
10^4	90,000	47.35	312.24	4,659.87

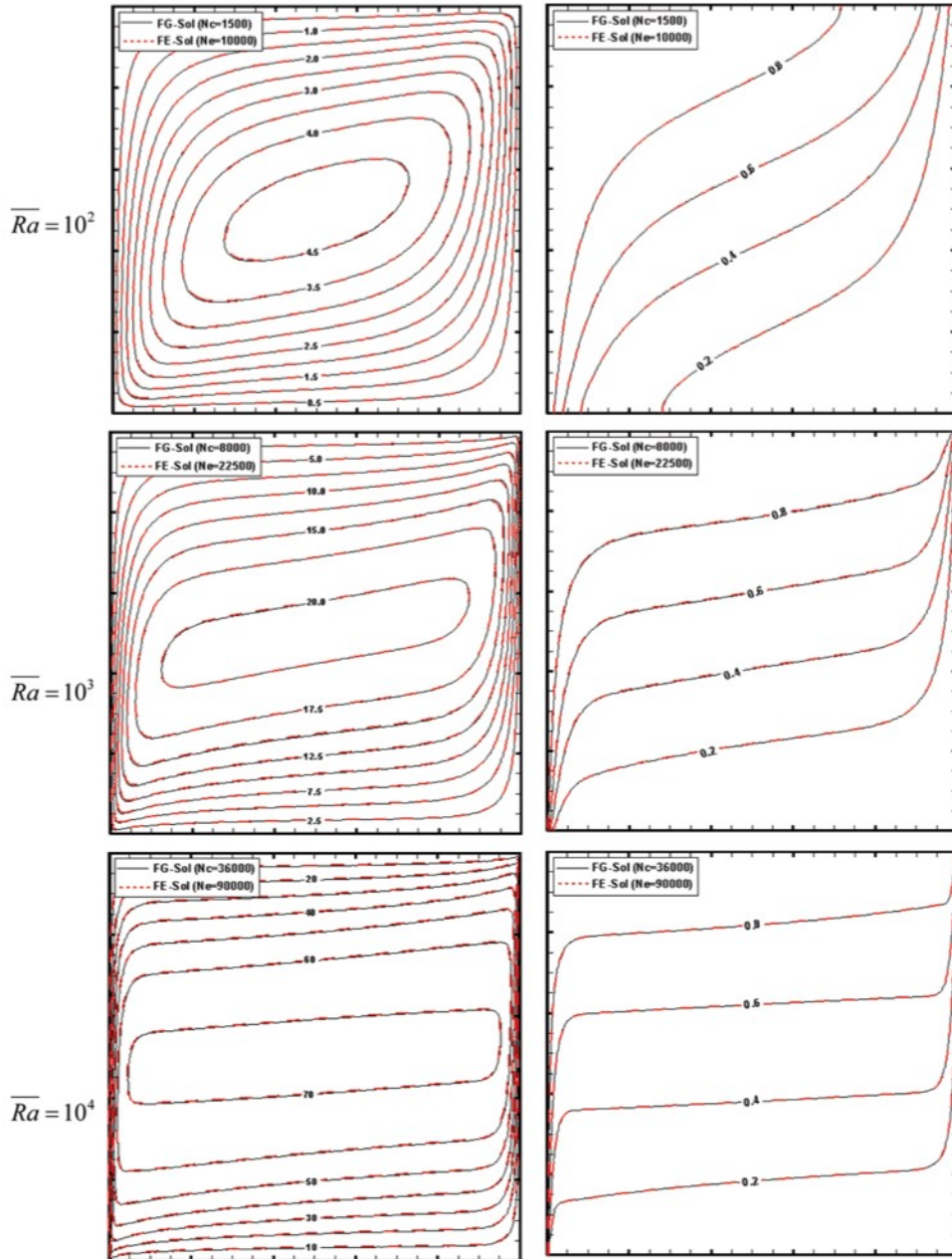


Figure 2. Streamlines and isotherms in the case of homogenous porous media ($\zeta = \sigma = 0$).

in the central region. This flow promotes heating near the top and cooling near the bottom of the cavity. For higher average Rayleigh numbers, the central low-velocity region expands horizontally and the flow region becomes confined to the walls (Figure 2).

Table 4. Comparison of the average Nusselt number ($\bar{\text{Nu}}$) with some published numerical results

Author	$\text{Ra} = 10^2$	$\text{Ra} = 10^3$	$\text{Ra} = 10^4$
Walker and Homsy [26]	3.09	12.96	51.00
Bejan [27]	4.20	15.80	50.80
Gross et al. [30]	3.14	13.44	42.58
Manole and Lage [33]	3.11	13.63	48.11
Baytas [38]	3.16	14.06	48.33
Nawaf and Pop [39]	3.00	13.72	43.95
Present study FG	3.11	13.38	46.14
Present study FE	3.10	13.48	47.35

The obtained results are compared to those from the literature in terms of Nusselt number in Table 4. This table shows several discrepancies between the published numerical results, especially for high Rayleigh numbers, and points out the accuracy of the developed reference solution.

5.2. Heterogeneous Cavity with Vertical Stratification

In this section, the permeability is assumed to be heterogeneous with $k(X, Z) = k_0 e^{\varsigma L X}$. Two levels of heterogeneity are studied corresponding to $\varsigma = 2$ and $\varsigma = 4$. The value of k_0 is calculated to be $3.13 \times 10^{-10} \text{ m}^2$ for $\varsigma = 2$ and $7.46 \times 10^{-11} \text{ m}^2$ for $\varsigma = 4$ to satisfy $\int_0^1 \int_0^1 k(X, Z) dX dZ = \bar{k}$. As in the previous test case, the reference solution is investigated for three values of the average Rayleigh number ($\bar{\text{Ra}} = 10^2$, 10^3 , and 10^4).

The results of the FG method are summarized in Table 5. This table gives the number of Fourier coefficients required to obtain the converged solution, the average Nusselt number, and the maximum velocities for the two heterogeneity levels. The results in this table show that the truncation order required to obtain a converged solution for a given average Rayleigh number increases with the level of heterogeneity. Indeed, for $\bar{\text{Ra}} = 10^3$, for example, the number of Fourier coefficients is 8,000 for the homogenous case. This number increases to 9,600 for the heterogeneous solution with $\varsigma = 2$, and to 16,000 with $\varsigma = 4$. This phenomenon is caused by the effects of the heterogeneity which increase the Rayleigh number locally and induces a solution that can be locally steeper and rougher than for the homogenous case.

Table 5. FG results in the case of vertical heterogeneity

$\bar{\text{Ra}}$	N_c	N_m	N_n	N_r	N_s	$\bar{\text{Nu}}$	U^{\max}	V^{\max}
$\varsigma = 2; \sigma = 0$								
10^2	2,000	25	40	24	40	2.63	17.22	44.77
10^3	9,600	60	80	59	80	10.84	92.55	348.22
10^4	44,200	130	170	129	170	37.64	493.15	3,440.66
$\varsigma = 4; \sigma = 0$								
10^2	3,000	30	50	29	50	1.88	12.46	45.18
10^3	16,000	80	100	79	100	6.24	79.20	200.48
10^4	50,400	140	180	139	180	21.52	487.45	1,376.14

Table 6. FE results in the case of vertical heterogeneity

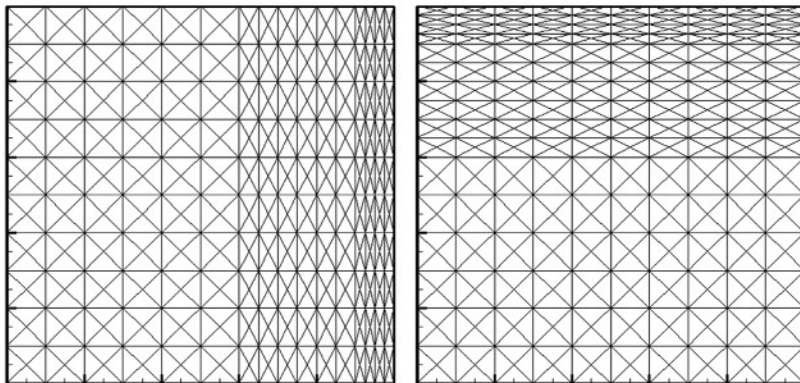
Ra	Ne	Nu	U^{\max}	V^{\max}
		$\zeta = 2; \sigma = 0$		
10^2	22,500	2.63	17.32	44.78
10^3	62,500	10.80	93.32	352.29
10^4	89,400 ^a	37.63	484.85	3,360.54
		$\zeta = 4; \sigma = 0$		
10^2	22,500	1.88	12.45	44.75
10^3	62,500	6.22	80.53	202.41
10^4	92,400 ^a	21.26	477.10	1,338.25

^aAdaptive mesh.

The numerical results obtained with the FE model are summarized in Table 6. The spatial discretization required to reach the converged numerical solution is highly dependent on the degree of heterogeneity. For example, for $\text{Ra} = 10^2$ and 10^3 , the number of mesh elements required to obtain the converged solution is greater than that for the homogenous solutions. Moreover, a special irregular mesh is used to obtain the converged FE solution for $\text{Ra} = 10^4$. This mesh involves local refinement on the high-permeability zones where the buoyancy effects are more significant (Figure 3a).

The results in Tables 5 and 6 show excellent agreement between the FG and the FE solutions. Indeed, for all the Rayleigh numbers, the difference between the FG and the FE results is less than 3%. These tables also show that the level of heterogeneity considerably affects the overall rate of heat transfer. The average Nusselt number decreases as the level of heterogeneity increases. Indeed, high heterogeneity levels produce low permeability near the hot wall and consequently reduce the convection process compared to the conduction one.

The simulated isotherms and streamlines are depicted in Figures 4 and 5 for $\zeta = 2$ and $\zeta = 4$, respectively. These figures show excellent agreement between the FG and FE results for all the values of average Rayleigh numbers. In addition, they

**Figure 3.** Irregular mesh for vertical and horizontal heterogeneity problems.

show that, because of the heterogeneity, the slow-motion region expands vertically and moves up toward the right corner, while the hot region becomes confined to the top surface of the porous cavity near the hot wall.

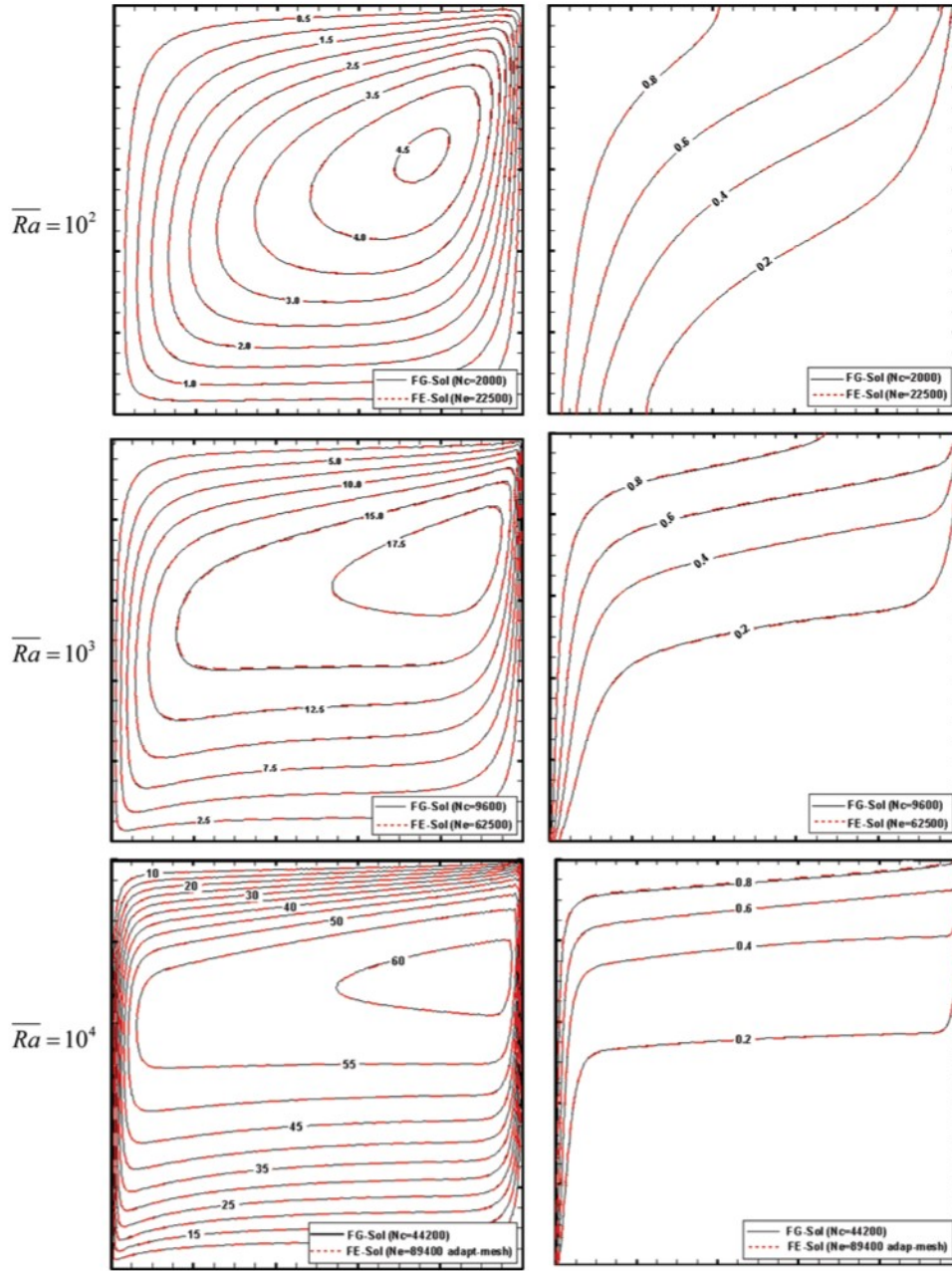


Figure 4. Streamlines and isotherms in the case of vertical heterogeneity ($\zeta=2$, $\sigma=0$).

5.3. Heterogeneous Cavity with Horizontal Stratification

In this section, the permeability is assumed to be heterogeneous with $k(X, Z) = k_0 e^{\sigma LZ}$. This leads to a horizontally stratified domain. As for the vertical case,

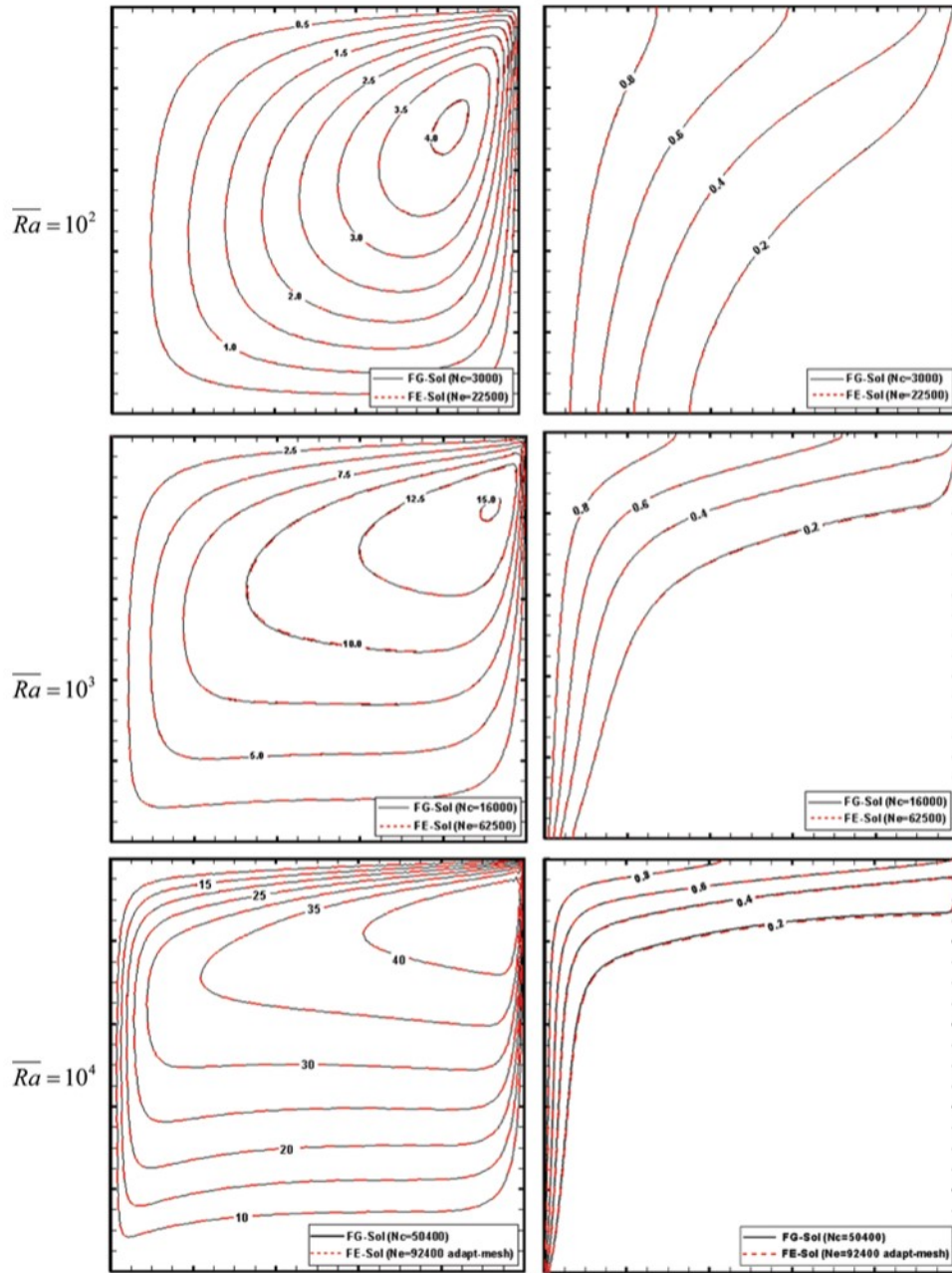


Figure 5. Streamlines and isotherms in the case of vertical heterogeneity ($\zeta=4$, $\sigma=0$).

Table 7. FG results in the case of horizontal heterogeneity

\bar{Ra}	Nc	Nm	Nn	Nr	Ns	\bar{Nu}	U^{\max}	V^{\max}
$\zeta=0; \sigma=2$								
10^2	2,000	25	40	24	40	2.93	30.18	37.35
10^3	16,000	80	100	79	100	13.29	135.81	497.11
10^4	50,400	140	180	139	180	47.38	595.29	5,188.46
$\zeta=0; \sigma=4$								
10^2	3,000	30	50	49	50	2.53	42.09	25.39
10^3	24,000	100	120	119	120	12.44	202.02	384.32
10^4	60,000	150	200	149	200	47.70	869.06	3,987.52

two levels of heterogeneity corresponding to $\sigma=2$ and $\sigma=4$ are considered. The values of k_0 are calculated to be $3.13 \times 10^{-10} \text{ m}^2$ and $7.46 \times 10^{-11} \text{ m}^2$ respectively. These values lead to the same average permeability as in the homogenous case. Similarly, the reference solution is investigated for three values of the average Rayleigh number ($\bar{Ra} = 10^2$, 10^3 , and 10^4). The corresponding FG results are given in Table 7. The number of Fourier coefficients required to obtain the converged solution is greater than that for the homogenous cases and that for the vertical heterogeneous cases. The FE results (Table 8) show that the horizontal heterogeneity renders the problem very sensitive to the computational mesh size. The number of mesh elements required to obtain the converged FE solution is greater than previously, especially with high Rayleigh numbers. Nonuniform grid involving mesh refinement in high-permeability regions (as in Figure 3b) are used to achieve convergence of the FE solution for $\bar{Ra} = 10^4$ with both levels of heterogeneity.

Excellent agreement between the converged FG and FE solutions can be observed in Tables 7 and 8. Indeed, for all the Rayleigh numbers, the difference between the FG and the FE results is less than 3%. These tables also show that for the horizontal stratification, the average Nusselt number is slightly sensitive to the vertical heterogeneity level.

Figures 6 and 7 show the obtained streamlines and isotherms. As for the previous cases, excellent agreement is reported between the FG and FE solutions.

Table 8. FE results in the case of horizontal heterogeneity

\bar{Ra}	Ne	\bar{Nu}	U^{\max}	V^{\max}
$\zeta=0; \sigma=2$				
10^2	22,500	2.93	30.40	37.24
10^3	90,000	13.20	136.95	485.50
10^4	92,400 ^a	46.35	579.49	5,041.36
$\zeta=0; \sigma=4$				
10^2	22,500	2.53	42.49	25.21
10^3	90,000	12.23	203.76	375.42
10^4	96,000 ^a	46.95	845.01	3,875.42

^aAdaptive mesh.

For this configuration, the streamlines show that the slow-motion region expands horizontally and moves up toward the right corner, while the isotherms show that the hot region becomes confined to the top surface of the domain.

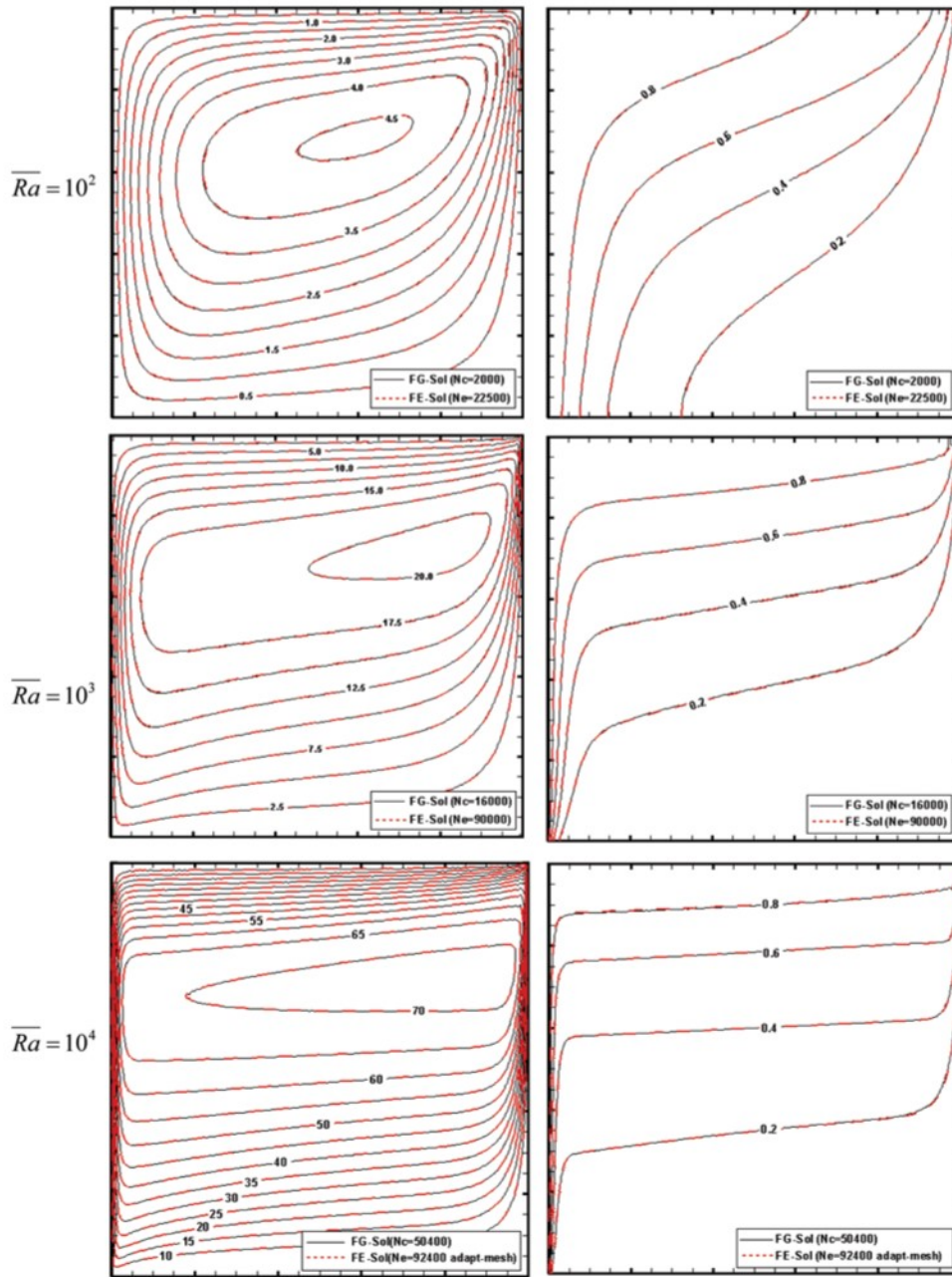


Figure 6. Streamlines and isotherms in the case of horizontal heterogeneity ($\xi=0, \sigma=2$).

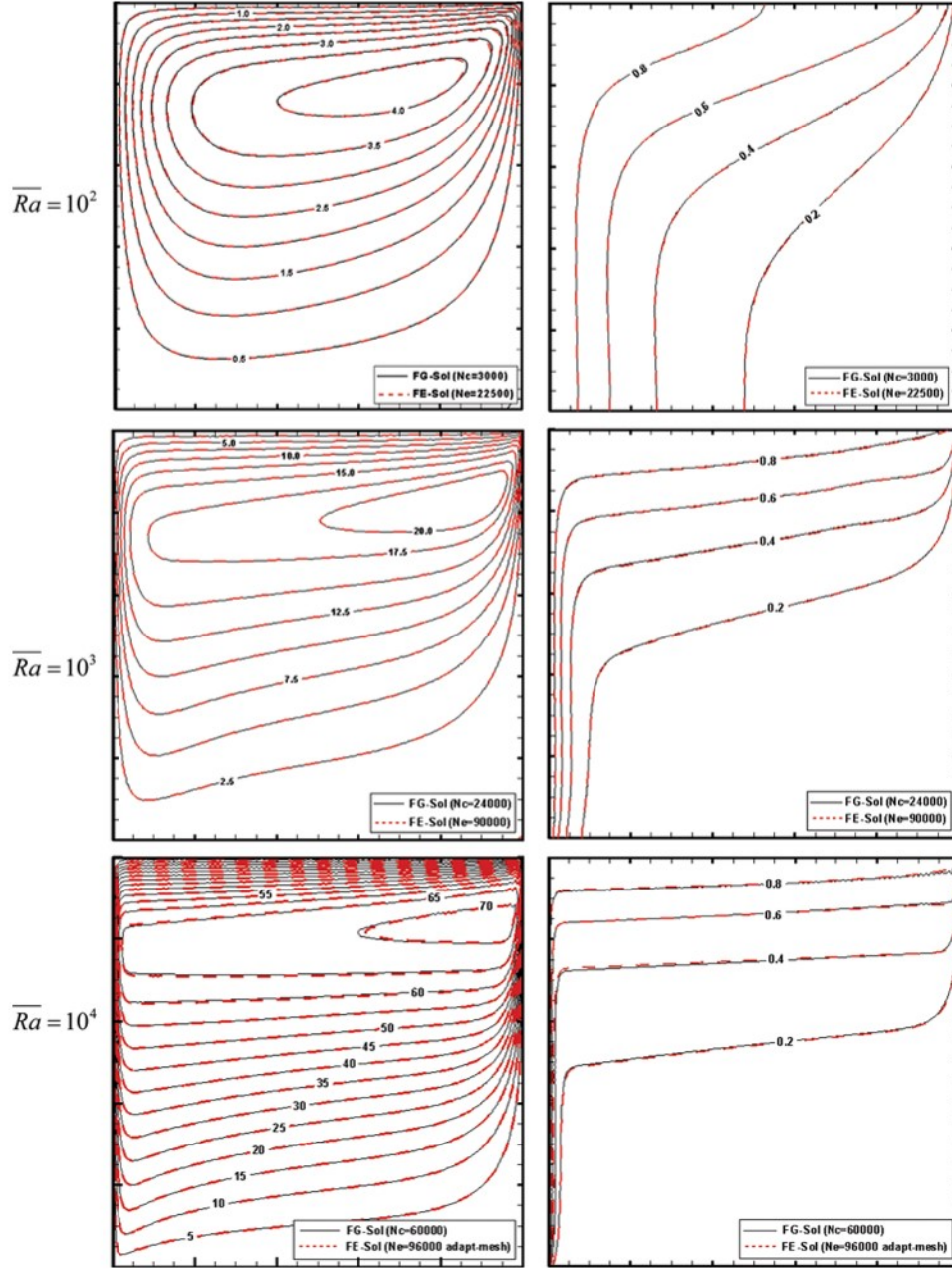


Figure 7. Streamlines and isotherms in the case of horizontal heterogeneity ($\xi = 0$, $\sigma = 4$).

6. SUMMARY AND CONCLUSION

In this study, reference solutions were developed for free convection in a heterogeneous porous cavity using the Fourier-Galerkin (FG) method. To this end, the

stream function and the temperature were expanded in a double set of Fourier series truncated at given orders. The resulting highly nonlinear system of algebraic equations was solved using the modified Powell's algorithm with an analytical evaluation of the Jacobian matrix. The reference solutions were validated by comparing the FG results to those of an accurate FE model based on advanced spatial and temporal discretization methods. The comparison between the FG and FE solutions was based on several quantities related to the velocity field (maximum velocity components and streamlines) and to the temperature distribution (average Nusselt number and isotherms).

Three configurations were investigated, corresponding to homogenous and vertically and horizontally stratified heterogeneous porous media with an exponential distribution of the permeability. For each configuration the free-convection problem was studied for three average Rayleigh numbers corresponding to 10^2 , 10^3 , and 10^4 .

For all the configurations, the number of Fourier coefficients (resp. mesh elements) required to obtain the converged FG (resp. FE) solution increases significantly for high Rayleigh numbers.

For the homogenous porous media, the streamlines indicate clockwise circulating flow with a relatively slow motion in the central region. The isotherms show a symmetric distribution of the hot and cold regions in the domain. The results from the literature for this configuration show several discrepancies, especially for large Rayleigh numbers. The obtained FG solution is in very good agreement with the converged FE solution and can therefore be considered as a reference solution for this configuration.

For the vertical and horizontal heterogeneous configurations, two levels of heterogeneity were studied. For both configurations, larger numbers of Fourier coefficients are required to obtain the converged solution for the higher heterogeneity level. Compared to the homogeneous configuration, finer meshes with local refinement were required to obtain the converged FE solution, especially for high average Rayleigh number.

For the vertical heterogeneity porous media, the streamlines and the isotherms are substantially affected by the heterogeneity. In this configuration, the slow-motion region moves up toward the cold wall and expands vertically. The temperature distribution gradually loses its symmetry, and the hot region becomes confined to the top surface of the square. The average Nusselt number is also considerably affected by the heterogeneity; it decreases when the level of heterogeneity increases.

For the horizontal stratification, the slow-motion region also moves up toward the cold wall. However, this region becomes horizontally expanded. The hot region becomes confined to the top surface of the domain. In this configuration, the average Nusselt number is slightly affected by the heterogeneity.

For both vertical and horizontal stratifications and for the low and high levels of heterogeneity, excellent agreement was found between the FG and FE converged solutions for all the quantities of interest. The newly developed solutions can therefore be used as reference solutions for free convection in heterogeneous porous media.

FUNDING

Ahmed Makradi acknowledges the financial support of the Fond National de la Recherche (FNR) of Luxembourg via FNR-CORE 2010 project OMIDEF (Grant FNR/786 643).

REFERENCES

1. D. B. Ingham and I. Pop, *Transport Phenomena in Porous Media*, vol. II Pergamon, Oxford, 2002.
2. D. A. Nield and A. Bejan, *Convection in Porous Media*, 2d ed., Springer-Verlag, New York, 1999.
3. I. Pop and D. B. Ingham, *Convective Heat Transfer: Mathematical and Computational Modelling of Viscous Fluids and Porous Media*, Elsevier Science & Technology Books, 2001.
4. D. Getachew, W. J. Minkowycz, and D. Poulikakos, Natural Convection in a Porous Cavity Saturated with a Non-Newtonian Fluid, *J. Thermophys. Heat Transfer*, vol. 10, pp. 640–651, 1996.
5. P. Vadasz, Bifurcation Phenomena in Natural Convection in Porous Media, *Heat Transfer*, Hemisphere, Washington, DC, vol. 5, pp. 147–152, 1990.
6. C. Braester and P. Vadasz, The Effect of a Weak Heterogeneity of a Porous Medium on natural convection, *J. Fluid Mech.*, vol. 254, pp. 345–362, 1993.
7. C. T. Simmons, T. R. Fenstemaker, and J. M. Sharp, Variable-Density Flow, and Solute Transport in Heterogeneous Porous Media: Approaches, Resolutions and Future Challenges, *J. Contam. Hydrol.*, vol. 52, pp. 245–275, 2001.
8. J. C. Leong and F. C. Lai, Effective Permeability of a Layered Porous Cavity, *ASME J. Heat Transfer*, vol. 123, pp. 512–519, 2001.
9. A. Prasad, and C. T. Simmons, Unstable Density-Driven Flow in Heterogeneous Porous Media: A Stochastic Study of the Elder [1967b] “Short Heater” Problem, *Water Resource Res.*, vol. 39, doi: 10.1029/2002WR001290, 2003.
10. J. C. Leong and F. C. Lai, Natural Convection in Rectangular Layers Porous Cavities, *J. Thermophys. Heat Transfer*, vol. 18, pp. 457–463, 2004.
11. D. A. Nield and A. Bejan, *Convection in Porous Media*, 3d ed., Springer-Verlag, New York, 2006.
12. D. A. Nield and C. T. Simmons, A Discussion on the Effect of Heterogeneity on the Onset of Convection in a Porous Medium, *Transp. Porous Media*, vol. 68, pp. 413–421, 2007.
13. D. A. Nield and A. V. Kuznetsov, The Effect of Combined Vertical and Horizontal Heterogeneity on the Onset of Convection in a Bidisperse Porous Medium, *Int. J. Heat Mass Transfer*, vol. 50, pp. 3329–3339, 2007.
14. D. A. Nield and A. V. Kuznetsov, The Effects of Combined Horizontal and Vertical Heterogeneity and Anisotropy on the Onset of Convection in a Porous Medium, *Int. J. Thermal Sci.*, vol. 46, pp. 1211–1218, 2007.
15. D. A. Nield and A. V. Kuznetsov, The Effects of Combined Horizontal and Vertical Heterogeneity on the Onset of Convection in a Porous Medium: Moderate Heterogeneity, *Int. J. Heat Mass Transfer*, vol. 51, pp. 2361–2367, 2008.
16. A. V. Kuznetsov and D. A. Nield, The Effects of Combined Horizontal and Vertical Heterogeneity on the Onset of Convection in a Porous Medium: Double Diffusive Case, *Transp. Porous Media*, vol. 72, pp. 157–170, 2008.
17. D. A. Nield, General Heterogeneity Effects on the Onset of Convection in a Porous Medium, in P. Vadasz (ed.), *Emerging Topics in Heat and Mass Transfer in Porous Media*, Springer-Verlag, chap. 3, 2008.
18. D. A. Nield, A. V. Kuznetsov, and C. T. Simmons, The Effect of Strong Heterogeneity on the Onset of Convection in a Porous Medium Non-periodic Global Variation, *Transp. Porous Media*, vol. 77, pp. 169–186, 2009.
19. A. V. Kuznetsov and D. A. Nield, The Effects of Combined Horizontal and Vertical Heterogeneity on the Onset of Convection in a Porous Medium with Vertical Through Flow, *Transp. Porous Media*, vol. 90, pp. 465–478, 2011.

20. K. Choukairy and R. Bennacer, Numerical and Analytical Analysis of the Thermosolutal Convection in an Heterogeneous Porous Cavity, *Tech Science Press FDMP*, vol. 8, pp. 155–172, 2012.
21. D. A. Nield and A. V. Kuznetsov, The Effect of Heterogeneity on the Onset of Double-Diffusive Convection Induced by Internal Heating in a Porous Medium: A Layered Model, *Transp. Porous Media*, vol. 100, pp. 83–99, 2013.
22. A. V. Kuznetsov and D. A. Nield, The Effect of Strong Heterogeneity on the Onset of Convection Induced by Internal Heating in a Porous Medium: A Layered Model, *Transp. Porous Media*, vol. 99, pp. 85–100, 2013.
23. D. A. Nield and A. V. Kuznetsov, Onset of Convection with Internal Heating in a Weakly Heterogeneous Porous Medium, *Transp. Porous Media*, vol. 98, pp. 543–552, 2013.
24. E. Holzbecher, Numerical Studies on Thermal Convection in Cold Groundwater, *Int. J. Heat Mass Transfer*, vol. 40, pp. 605–612, 1997.
25. E. Holzbecher, The Fast-C Simulators for Density-Driven Flow: Application to Geothermal Modelling, *Proc. World Geothermal Congress*, Kyushu-Tohoku, Japan, 2000.
26. K. L. Walker and G. M. Homsy, Convection in a Porous Cavity, *J. Fluid Mech.*, vol. 87, pp. 449–474, 1978.
27. A. Bejan, On the Boundary Layer Regime in a Vertical Enclosure Filled with a Porous Medium, *Lett. Heat Mass Transfer*, vol. 6, pp. 93–102, 1979.
28. G. Schubert and J. M. Straus, Transitions in Time-Dependent Thermal Convection in Fluid-Saturated Porous Media, *J. Fluid Mech.*, vol. 121, pp. 301–313, 1982.
29. V. Prasad and F. A. Kulacki, Convective Heat Transfer in a Rectangular Porous Cavity—Effect of Aspect Ratio on Flow Structure and Heat Transfer, *J. Heat Transfer*, vol. 106, pp. 158–165, 1984.
30. R. J. Gross, M. R. Bear, and C. E. Hickox, The Application of Flux-Corrected Transport (FCT) to high Rayleigh Number Natural Convection in a Porous Medium, *Proc. 8th International Heat Transfer Conference*, San Francisco, CA, 1986.
31. V. Prasad and A. Tuntomo, Inertia Effects on Natural Convection in a Vertical Porous Cavity, *Numer. Heat Transfer B*, vol. 11, pp. 295–320, 1987.
32. R. Rajamani, C. Srinivas, and K. N. Seetharamu, Finite Element Analysis of Convection Heat Transfer in Porous Media, *Int. J. Numer. Meth. Fluids*, vol. 11, pp. 331–339, 1990.
33. D. M. Manole and J. L. Lage, Numerical Benchmark Results for Natural Convection in a Porous Medium Cavity, *HTD Heat and Mass Transfer in Porous Media, ASME Conference*, vol. 216, pp. 55–60, 1992.
34. C. Baohua and R. M. Cotta, Integral Transform Analysis of Natural Convection in Porous Enclosures, *Int. J. Numer. Meth. Fluids*, vol. 17, pp. 787–801, 1993.
35. D. Misra and A. Sarkar, A Comparative Study of Porous Media Models in a Differentially Heated Square Cavity Using a Finite Element Method, *Int. J. Numer. Meth. Heat Fluid Flow*, vol. 5, pp. 735–752, 1995.
36. E. Holzbecher, *Modeling Density-Driven Flow in Porous Media: Principles, Numerics, Software*, Springer-Verlag, Heidelberg-New York, 1998.
37. L. S. de B. Alves and R. M. Cotta, Transient Natural Convection inside Porous Cavities: Hybrid Numerical-Analytical Solution and Mixed Symbolic-Numerical Computation, *Numer. Heat Transfer A*, vol. 38, pp. 89–110, 2000.
38. A. C. Baytas, Entropy Generation for Natural Convection in an Inclined Porous Cavity, *Int. J. Heat Mass Transfer*, vol. 43, pp. 2089–2099, 2000.
39. H. S. Nawaf and I. Pop, Transient Free Convection in a Square Cavity Filled with a Porous Medium, *Int. J. Heat Mass Transfer*, vol. 47, pp. 1917–1924, 2004.
40. H. Luz Neto, J. N. N. Quaresma, and R. M. Cotta, Integral Transform Solution for Natural Convection in Three-Dimensional Porous Cavities: Aspect Ratio Effects, *Int. J. Heat Mass Transfer*, vol. 49, pp. 4687–4695, 2006.

41. H. R. Henry, Effects of Dispersion on Salt Encroachment in Coastal Aquifers, in Sea Water in Coastal Aquifers, *U.S. Geol. Surv. Supply Pap.*, vol. 1613, pp. 70–84, 1964.
42. D. Durran, *Numerical Methods for Wave Equations in Geophysical Fluid Dynamics*, chap. 4, Springer-Verlag, New York, 1999.
43. B. Costa, Spectral Methods for Partial Differential Equations, *Cubo Math. J.*, vol. 6, pp. 1–32, 2004.
44. M. Christou and C. I. Christov, Fourier-Galerkin Method for Localized Solutions of Equations with Cubic Nonlinearity, *J. Comput. Anal. Appl.*, vol. 4, pp. 63–77, 2002.
45. M. A. Christou and C. I. Christov, Fourier-Galerkin Method for Interacting Localized Waves, *J. Neural Parallel Sci. Comput.*, vol. 4, pp. 63–77, 2002.
46. M. A. Christou and C. I. Christov, Localized Waves for the Regularized Long Wave Equation via a Galerkin Spectral Method, *Math. Comput. Simul.*, vol. 69, pp. 257–268, 2005.
47. C. Canuto, M. Hussaini, A. Quarteroni, and T. Zang, *Spectral Methods: Fundamentals in Single Domains*, chap. 3, Springer-Verlag, New York, 2006.
48. M. Christou and C. I. Christov, Fourier-Galerkin Method for 2D Solutions of Boussinesq Equation, *Math. Comput. Simul.*, vol. 74, pp. 82–92, 2007.
49. D. A. Kopriva, *Implementing Spectral Methods for Partial Differential Equations*, chap. 4, Springer Science, New York, 2009.
50. A. Zidane, A. Younes, P. Huggenberger, and E. Zechner, The Henry Semi-Analytical Solution for Saltwater Intrusion with Reduced dispersion, *Water Resources Res.*, vol. 48, pp. 1–10, 2012.
51. M. Fahs and A. Younes, A High Accurate Fourier-Galerkin Solution for Buoyancy-Driven Flow in a Square Cavity, *J. of Numer. Heat Transfer B*, vol. 65, pp. 495–517, 2014.
52. M. Y. Hussaini and T. A. Zang, Spectral Methods in Fluid Dynamics, *Annu. Rev. Fluid Mech.*, vol. 19, pp. 339–367, 1987.
53. K. Hooman, Heat and Fluid Flow in a Rectangular Microchannel Filled with a Porous Medium, *Int. J. Heat Mass Transfer*, vol. 51, pp. 5804–5810, 2008.
54. M. A. Christou and C. I. Christov, Interacting Localized Waves for the Regularized Long Wave Equation via a Galerkin Spectral Method, *Math. Comput. Simul.*, vol. 69, pp. 257–268, 2005.
55. M. J. D. Powell, An Efficient Method for Finding the Minimum of a Function of Several Variables without Calculating Derivatives, *Comput. J.*, vol. 7, pp. 155–162, 1964.
56. M. J. D. Powell, On the Calculations of Orthogonal Vectors, *Comput. J.*, vol. 1, pp. 302–304, 1968.
57. W. H. Press, S. A. Teukolsky, W. T. Vetterling, and B. P. Flannery, *Numerical Recipes: The Art of Scientific Computing*, 3d ed., chap. 9–10, Cambridge University Press, New York, 2007.
58. A. Younes, M. Fahs, and S. Ahmed, Solving Density Driven Flow Problems with Efficient Spatial Discretizations and Higher-Order Time Integration Methods, *Adv. Water Res.*, vol. 32, pp. 340–352, 2009.
59. A. Younes and P. Ackerer, Solving the Advection–Dispersion Equation with Discontinuous Galerkin and Multipoint Flux Approximation Methods on Unstructured Meshes, *Int. J. Numer. Meth. Fluids*, vol. 58, pp. 687–708, 2008.
60. S. Mahmud and I. Pop, Mixed Convection in a Square Vented Enclosure Filled with a Porous Medium, *Int. J. Heat Mass Transfer*, vol. 49, pp. 2190–2206, 2006.
61. IMSL. Math/Library, Visual Numerics, Houston, TX, 1997.
62. C. G. Broyden, A Class of Methods for Solving Nonlinear Simultaneous Equations, *Math. Comput.*, vol. 19, pp. 577–593, 1965.

63. M. W. Farthing, C. E. Kees, and C. T. Miller, Mixed Finite Element Methods and Higher Order Temporal Approximations, *Adv. Water Res.*, vol. 25, pp. 85–101, 2002.
64. L. Durlofsky, Accuracy of Mixed and Control Volume Finite Element Approximations to Darcy Velocity and Related Quantities, *Water Resources Res.*, vol. 30, pp. 965–73, 1994.
65. T. Shuangzhang and A. Shahrouz, A Slope Limiting Procedure in Discontinuous Galerkin Finite Element Method for Gas Dynamics Applications, *Int. J. Numer. Anal. Model.*, vol. 2, pp. 163–78, 2005.
66. A. Younes and V. Fontaine, Hybrid and Multi Point Formulations of the Lowest Order Mixed Methods for Darcy's Flow on Triangles, *Int. J. Numer. Meth. Fluids*, vol. 58, pp. 1041–1062, 2008.
67. A. C. Hindmarsh, LSODE and LSODI, Two New Initial Value Ordinary Differential Equation Solvers, *SIGNUM Newslett.*, vol. 15, pp. 10–11, 1980.
68. A. C. Hindmarsh, Large Ordinary Differential Equation Systems and Software, *IEEE Cont. Sys. Mag.*, vol. 2, pp. 24–30, 1982.
69. A. C. Hindmarsh, ODEPACK: A Systematized Collection of ODE Solvers, R. S. Stepleman et al. (ed.), *Scientific Computing*, p. 55–64.; North-Holland, Amsterdam, 1983.
70. A. C. Hindmarsh, The ODEPACK Solvers, R. C. Aiken, (ed.), *Stiff Computation*, pp. 167–174, Oxford University Press, 1985.

APPENDIX: DEVELOPMENT OF THE FOUR-OVERLAPPED-SUMMATIONS TERM

The term involving four overlapped summations can be written as the summation of the following two subterms:

$$\text{Term1}_{g,h} = \sum_{m=1}^{Nm} \sum_{n=1}^{Nn} \sum_{r=0}^{Nr} \sum_{s=1}^{Ns} A_{m,n} B_{r,s} (m.s.\gamma_{g,m,r}\lambda_{h,n,s}) \quad (\text{A.1})$$

$$\text{Term2}_{g,h} = \sum_{m=1}^{Nm} \sum_{n=1}^{Nn} \sum_{r=0}^{Nr} \sum_{s=1}^{Ns} A_{m,n} B_{r,s} (n.r.\tau_{g,m,r}\xi_{h,n,s}) \quad (\text{A.2})$$

Using the expressions of the coefficients γ and λ as given in Eq. (26), Eq. (A.1) can be written as follows:

$$\begin{aligned} \text{Term1}_{g,h} = & \sum_{m=1}^{Nm} \sum_{n=1}^{Nn} \sum_{r=0}^{Nr} \sum_{s=1}^{Ns} m.s.A_{m,n} B_{r,s} \delta_{g,m-r} \delta_{h,n+s} \\ & + \sum_{m=1}^{Nm} \sum_{n=1}^{Nn} \sum_{r=0}^{Nr} \sum_{s=1}^{Ns} m.s.A_{m,n} B_{r,s} \delta_{g,m-r} \delta_{h,n-s} \\ & - \sum_{m=1}^{Nm} \sum_{n=1}^{Nn} \sum_{r=0}^{Nr} \sum_{s=1}^{Ns} m.s.A_{m,n} B_{r,s} \delta_{g,m-r} \delta_{h,s-n} \\ & + \sum_{m=1}^{Nm} \sum_{n=1}^{Nn} \sum_{r=0}^{Nr} \sum_{s=1}^{Ns} m.s.A_{m,n} B_{r,s} \delta_{g,r-m} \delta_{h,n+s} \\ & + \sum_{m=1}^{Nm} \sum_{n=1}^{Nn} \sum_{r=0}^{Nr} \sum_{s=1}^{Ns} m.s.A_{m,n} B_{r,s} \delta_{g,r-m} \delta_{h,n-s} \end{aligned}$$

$$\begin{aligned}
& - \sum_{m=1}^{Nm} \sum_{n=1}^{Nn} \sum_{r=0}^{Nr} \sum_{s=1}^{Ns} m.s.A_{m,n}B_{r,s}\delta_{g,r-m}\delta_{h,s-n} \\
& + \sum_{m=1}^{Nm} \sum_{n=1}^{Nn} \sum_{r=0}^{Nr} \sum_{s=1}^{Ns} m.s.A_{m,n}B_{r,s}\delta_{g,m+r}\delta_{h,n+s} \\
& + \sum_{m=1}^{Nm} \sum_{n=1}^{Nn} \sum_{r=0}^{Nr} \sum_{s=1}^{Ns} m.s.A_{m,n}B_{r,s}\delta_{g,m+r}\delta_{h,n-s} \\
& - \sum_{m=1}^{Nm} \sum_{n=1}^{Nn} \sum_{r=0}^{Nr} \sum_{s=1}^{Ns} m.s.A_{m,n}B_{r,s}\delta_{g,m+r}\delta_{h,s-n}
\end{aligned} \tag{A.3}$$

Let us consider the first term in Eq. (A.3). Using the relations $\delta_{g, m-r} = \delta_{r, m-g}$ and $\delta_{h,n+s} = \delta_{h-n,s}$ and the property $\sum_i \sum_j \sum_k \sum_l A_{i,j}B_{k,l}\delta_{i,k}\delta_{j,l} = \sum_i \sum_j A_{i,j}B_{i,j}$, this term can be simplified to

$$\sum_{m=1}^{Nm} \sum_{n=1}^{Nn} \sum_{r=0}^{Nr} \sum_{s=1}^{Ns} m.s.A_{m,n}B_{r,s}\delta_{g,m-r}\delta_{h,n+s} = \sum_{m=1}^{Nm} \sum_{n=1}^{Nn} m.(h-n).A_{m,n}B_{m-g,h-n} \tag{A.4}$$

When the same procedure is applied to all the terms in Eq. (A.3), Term1_{g,h} can be written as follows:

$$\text{Term1}_{g,h} = \sum_{m=1}^{Nm} \sum_{n=1}^{Nn} m.A_{m,n} \left[(h-n)b_{m,n,g,h}^I + (n-h)b_{m,n,g,h}^H - b_{m,n,g,h}^{III}(h+n) \right] \tag{A.5}$$

where $b_{m,n,g,h}^I$, $b_{m,n,g,h}^H$, and $b_{m,n,g,h}^{III}$ are given by

$$b_{m,n,g,h}^I = (B_{m-g,h-n} + B_{g+m,h-n} + B_{g-m,h-n}) \tag{A.6}$$

$$b_{m,n,g,h}^H = (B_{m-g,n-h} + B_{g+m,n-h} + B_{g-m,n-h}) \tag{A.7}$$

$$b_{m,n,g,h}^{III} = (B_{m-g,h+n} + B_{g+m,h+n} + B_{g-m,h+n}) \tag{A.8}$$

The term Term2_{g,h} is simplified in the same manner. Hence, it can be written as follows:

$$\text{Term2}_{g,h} = \sum_{m=1}^{Nm} \sum_{n=1}^{Nn} n.A_{m,n} \left[b_{m,n,g,h}^{IV}(g+m) + b_{m,n,g,h}^V(m-g) - b_{m,n,g,h}^{VI}(g-m) \right] \tag{A.9}$$

where $b_{m,n,g,h}^{IV}$, $b_{m,n,g,h}^V$, and $b_{m,n,g,h}^{VI}$ are given by

$$b_{m,n,g,h}^{IV} = (B_{g+m,h-n} - B_{g+m,n-h} + B_{g+m,h+n}) \tag{A.6}$$

$$b_{m,n,g,h}^V = (B_{m-g,h-n} - B_{m-g,n-h} + B_{m-g,h+n}) \tag{A.7}$$

$$b_{m,n,g,h}^{VI} = (B_{g-m,h-n} - B_{g-m,n-h} + B_{g-m,h+n}) \tag{A.8}$$